

Article

Rapid Detection of Mercury Ions Using Sustainable Natural Gum-Based Silver Nanoparticles

Samie Yaseen Sharaf Zeebaree ^{1,*} , Osama Ismail Haji ^{2,3} , Aymn Yaseen Sharaf Zeebaree ¹ ,
Dunya Akram Hussein ¹ and Emad Hameed Hanna ¹

¹ Department of Medical Laboratory Technology, College of Health and Medical Technology, Duhok Polytechnic University, Kurdistan Region, Dahuk 42001, Iraq

² Medical Biochemical Analysis Department, College of Health Technology, Cihan University-Erbil, Kurdistan Region, Erbil 44008, Iraq

³ General Science Department, Faculty of Education, Soran University, Soran 44008, Iraq

* Correspondence: samie.yasin@dpu.edu.krd

Abstract: Fabrication of metal nanostructures using natural products has attracted scientists and researchers due to its renewable and environmentally benign availability. This work has prepared an eco-friendly, low-cost, and rapid colorimetric sensor of silver nanoparticles using tree gum as a reducing and stabilizing agent. Several characterization techniques have been exploited to describe the synthesized nanosensor morphology and optical properties. Ultraviolet–Visible (UV–Vis) spectroscopy has been used for monitoring the localized plasmon surface area. High-resolution transmission electron microscopy (HR-TEM) illustrated the size and shape of silver nanoparticles. X-ray diffraction spectra showed the crystallography and purity of the product. Silver nanoparticles decorated with almond gum molecules (AgNPs@AG) demonstrated high sensitivity and colorimetric detection of mercury ions in water samples. The method is based on the aggregation of AgNPs and the disappearing yellow color of AgNPs via a spectrophotometer. The detection limit of this method was reported to be 0.5 mg/L. This work aimed to synthesize a rapid, easy-preparation, eco-friendly, and efficient naked-eye colorimetric sensor to detect toxic pollutants in aqueous samples.

Keywords: natural gum; silver nanoparticles; mercury ion detection



Citation: Sharaf Zeebaree, S.Y.; Haji, O.I.; Zeebaree, A.Y.S.; Hussein, D.A.; Hanna, E.H. Rapid Detection of Mercury Ions Using Sustainable Natural Gum-Based Silver Nanoparticles. *Catalysts* **2022**, *12*, 1464. <https://doi.org/10.3390/catal12111464>

Academic Editors: Beom Soo Kim and Pritam Kumar Dikshit

Received: 13 August 2022

Accepted: 10 November 2022

Published: 18 November 2022

Publisher's Note: MDPI stays neutral with regard to jurisdictional claims in published maps and institutional affiliations.



Copyright: © 2022 by the authors. Licensee MDPI, Basel, Switzerland. This article is an open access article distributed under the terms and conditions of the Creative Commons Attribution (CC BY) license (<https://creativecommons.org/licenses/by/4.0/>).

1. Introduction

Population growth worldwide has led to increased demand for drinking water in recent years. However, water resources have suffered from pollution due to industrial sectors' discharging various kinds of pollutants and harmful substances. Many kinds of pollutants, such as herbicides, pesticides, dyes, plastics, oil derivatives, and heavy metals [1–4], have been found in water effluents, which is the main reason behind the development of health issues among people. Mercury and its compounds are among the most harmful species reported and adversely affect human health [5]. Mercury affects the central nervous system, liver, and kidney. Further, it can disturb the immune system due to impaired hearing, vision, paralysis, and emotional instability. Many analytical techniques are employed for detecting mercury ions, such as inductively coupled plasma atomic emission and mass spectroscopy, cold vapor atomic absorption spectroscopy, cold vapor atomic fluorescence spectroscopy, and high-performance liquid chromatography with UV–Vis detection [6]. However, these techniques suffer from several limitations, for instance, time consumption, harmful solvents, equipment costs, and complex procedures [7]. Therefore, developing new approaches to detecting and determining mercury ions becomes crucial and an urgent need.

Metal nanoparticles possess several unique optical, photothermal, and electrical properties. These distinctive characteristics make scientists more curious to investigate and uncover the potential applications of metal nanoparticles [8]. Gold, silver, and copper nanoparticles have been used widely in many fields such as medicine, industry, agriculture,

and the environment. The vast spectrum of applications of these nanostructured metals come from the nanoscale size, which has a variant behavior for its bulk state [9]. However, it must undergo chemical, physical, or biological processing to convert a metal from a bulk state to nanoscale particles. Biological methods are considered an emerging technique used to fabricate metal nanoparticles. It is classified into two main subclasses, that is, plant and microorganism. The plant's parts include roots, stems, flowers, leaves, and seeds [10]. Some trees' stems release exudate (gum) as a defense weapon against microorganisms and insects [11]. However, the gum has been proven to contain many active chemical components. Almond gum is a natural product released from the tree stem. It contains fats (0.85%), protein (2.45%), and carbohydrates (92.36%). Carbohydrates include glucose, galactose, arabinose, mannose, rhamnose, and uronic acid. These bioactive compounds possess active functional groups such as hydroxyl groups (OH), carboxylic groups (COOH), and carbonyl groups (CO). It is considered a rich site electron donor and has a crucial role in reducing action [12].

Prior studies have been performed to prepare silver nanoparticles using plant exudate. For instance, *Mimosa pudica* gum was successfully employed in the synthesis of silver nanoparticles as an antimicrobial agent [13]. Gum *Tragacanth* has been used as a reducing and stabilizing agent for fabricating silver nanoparticles [14]. The aqueous solution of gum *Acacia* was utilized efficiently in the preparation of silver nanoparticles [15]. Arabic gum has served a dual function for synthesizing silver nanoparticles and evaluating its activity against pathogen bacteria [16]. *Cashew* gum has been exploited for the production of silver nanoparticles to study its activity as an anti-bacterium [17]. Biogenic silver nanoparticles were prepared with gum *ghatti* and gum *olibanum*. Further, inhibition action against certain bacteria was observed and was biocompatible with other bacteria [18]. Catalytic activity has been evaluated in silver nanoparticles synthesized by gum *Karaya* [19]. Plant gums of *Araucaria heterophylla*, *Azadirachta indica*, and *Prosopis chilensis* mediated have been used for the fabrication of silver nanoparticles and assisted in the removal of heavy metal, anticancer, and antibacterial agents [20]. Most of the mentioned studies fabricated distinctive and efficient silver nanoparticles. However, they have used complex apparatuses, high temperature, high pressure, and long-time reactions. Further, they concentrated on biological applications.

The current study has employed almond gum as a reducing and capping agent to synthesize a eco-friendly, low-cost, easy-preparation and rapid naked eye colorimetric sensor for silver nanoparticles. Further, AgNps@AG showed rapid and high sensitivity to mercury (II) ions in an aqueous medium.

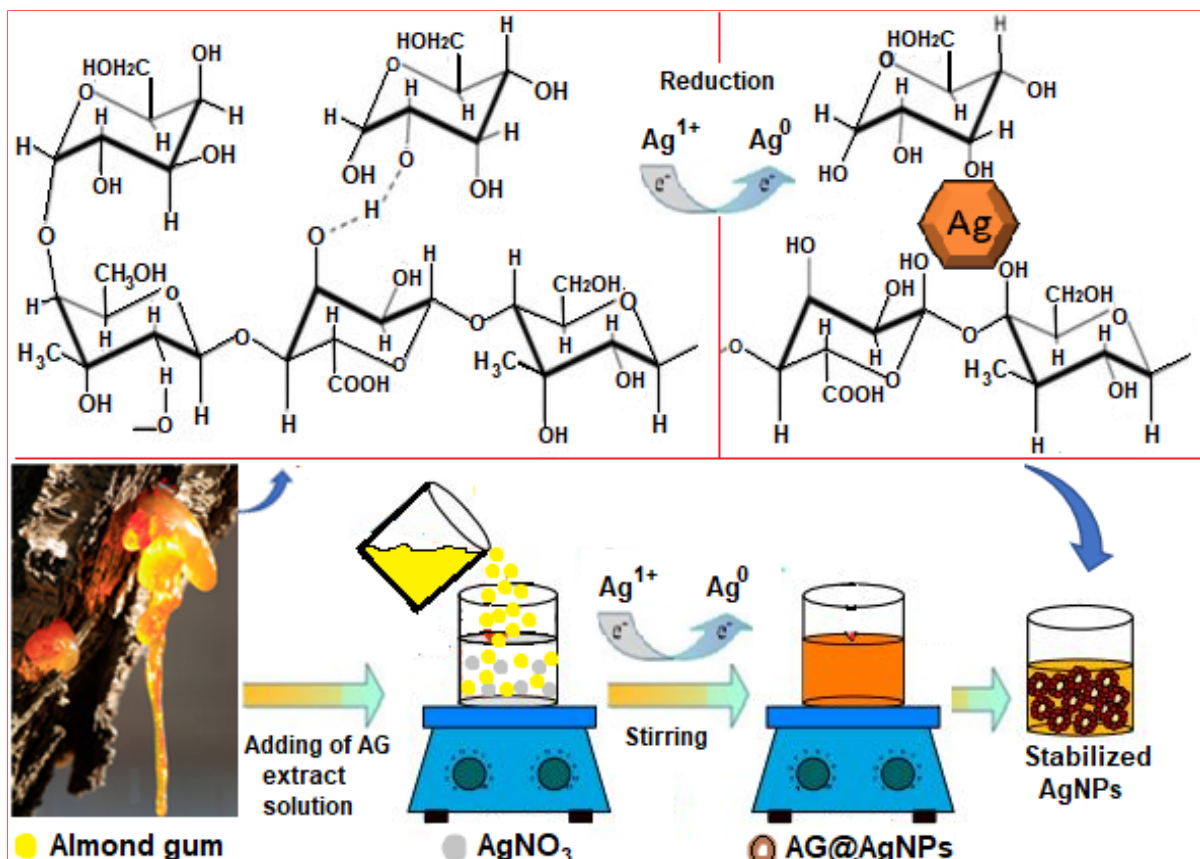
2. Results and Discussion

2.1. Fabrication of AgNPs@AG

Nanotechnology's essence is synthesizing nanoparticles according to simple, easy, inexpensive, and environmentally friendly steps, including the use of green natural resources. However, validating the principle of the synthesis of nanoparticles using bio-waste extracts, including plants, is considered to be of paramount importance in the scientific and research community. Over the past years, many green metallic nanoparticles, including copper, selenium, titanium, and silver, have been synthesized according to the green reduction mechanism through active biological components operating in plants. Most of the plant body comprises multiple vital compounds, such as proteins, carboxylic acids, flavonoids, glycosides, and polysaccharides, in addition to a percentage of metals and hydrating compounds. Due to its high biosignificance, the gum contents have been investigated by Hossein and Ali's group using HPLC and FTIR analysis [21]. The HPLC analysis revealed that the gum contains an excellent ratio of many active chemical compounds, such as proteins, polysaccharides, uronic acid, fats, and ash.

In contrast, the FTIR study for these compounds showed that their structures consist of various active functional groups such as C=O, CO₂H, OH, and NH₂. According to the analysis, the high value of the almond gum return to the polysaccharide, which involve

several monosaccharides such as rhamnose, mannose, glucose, xylose, arabinose, and galactose existing in the branched chain of structure. However, due to the foundation of hydroxy–flavonoid structure in these saccharides containing a high OH groups ratio, it is responsible for reducing many metal ions to nanoparticles. Therefore, the formation of AgNPs@AG can be attributed to the poly- and monosaccharides molecules, which are considered active chelating compounds because they possess multiple hydroxyl groups located at carbon atoms of the flavone rings (Scheme 1). This hypothesis has been confirmed by several published reports on reducing various metal ions, such as Cu^{2+} , Se^{2+} , Ti^{4+} , Fe^{3+} , and Zn^{2+} , using plant extracts [22].



Scheme 1. The supposed mechanism for the fabrication of AgNPs@AG by an almond gum extract.

2.2. UV–Vis Analysis Measurement

Employing ultra violet-visible spectroscopy to identify nanoparticles is a powerful and valuable method for the preliminary diagnosis of bio-fabricated AgNPs@AG. However, after mixing the required colorless components for the preparation of the AgNPs@AG catalyst, dark brown color was formed. The formation of this color was an initial confirmation of the synthesis of AgNPs@AG. Nevertheless, for more support, the observed color value of the catalyst was read on a nanodrop 2000/2000c spectrophotometer at the scale of 250–700 nm, where a robust and broad curve at 410 nm was recorded on the formation of nanoparticles with LSPR properties. The appearance of this result is a confirmation point on the formation of NPs in nanosizes, which agrees with a previous published report' data [23]. The brown–yellow color formation was returned to the reduction process between the Ag^+ ions and active functional groups present in the gum extract components and eventually formed Ag^0 . Moreover, it was due to the excitation of the surface plasmon resonance (SPR) vibrations of electrons in AgNPs (Figure 1—red line). The valence band and the conduction band of the AgNPs were very close, making a good reason for electrons moving freely, giving a sharp SPR absorption band at 410 nm [24]. In contrast, this band was monitored

after adding a brown–yellow sensor solution to the mercury ions sample (Figure 1—blue line). The analysis revealed excellent suppression for the sensor color to be colorless during 13 seconds at ambient conditions. Furthermore, this color’s disappearance and formation of a colorless phase were approved on the well unit of Ag with Hg ions to form a Ag–Hg phase in the aqueous solution. This result has been proven in many literature and research works [25].

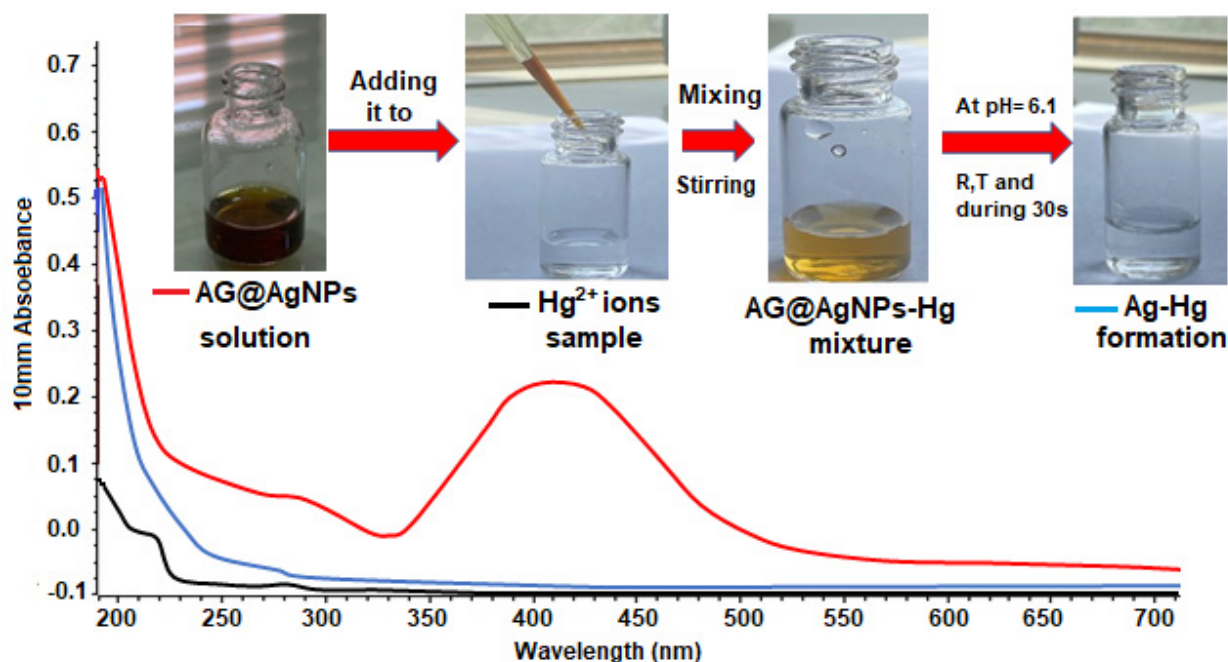


Figure 1. Measured UV–Vis spectra of Hg^{2+} (black line), AgNPs@AG (red line), and Ag–Hg (blue line).

2.3. Surface Morphology Diagnosis

Investigation of the oxidation states and nature of the surface of the prepared nanomaterials is crucial and widely needed in multiple applications and fields. For this requirement, XPs analysis was utilized to diagnose the orbitals type formed for AG surfaces and encapsulated AgNPs as well as the reaction mixture sample (AgNPs–Hg or Ag–Hg) as shown in Figure 2a,b. For the AG extract (Figure 2a—blue line), the XPS analysis chart showed two firm peaks located at binding energies of 283 and 539 eV, returning to the carbon atom (C 1s) and an oxygen atom (O 1s), respectively. However, the appearance of these atoms (i.e., C and O) are generally back to the presence of multi-organic compounds in gum bio content such as flavones, phenols, and carboxylic acids, which especially possess multi-functional groups in their structures such as C–C, C–O–C, C=O, OH, and COOH. The presence of these active groups came from the existence of hydroxyl and carbonyl groups that built the polymeric structure of polysaccharides. Additionally, these single bands (C 1s and O 1s) were extensive supports and evidence of the stability of cyclic C–C atoms of ketonic polysaccharides rings in the resin structure. The measured results of previous works strongly confirm the recorded data in this regard [26]. In contrast, after encapsulating the AG–Ag NPs by resin, the analysis survey of XPs (Figure 2a—black line) showed excellent three satellite peaks located at 288, 400, and 533 eV, respectively, which are attributed to the core levels of C 1s, Ag 3d, and O 1s, respectively. Noticing and recording these orbitals is a good indication of the coating of synthesized NPs by gum components. This diagnosis corresponds well with the previously published reports for the fabrication of a zerovalent silver state [27]. No presence or appearance of other elements in the spectrum analysis is a well proof of the use of almond gum as a sustainable reducing and stabilizing agent for designing silver nanosensors. However, the sensor activity for the prepared AgNPs@AG

was tested, and XPs analysis survey was applied to show the sensor efficiency in detecting Hg ions to prove the reaction process between AgNPs and Hg ions. XPs diagnosis for the mixture (Figure 2b—brown line) revealed significant photoelectron peaks values at 100 and 120 eV, which returned to the orbital states of Ag 3d5/2 and Hg 4f, respectively. These types of orbitals were formed due to the adsorption of mercury ions on the gum surface. The redox process by the transition of electrons between the Ag⁰ and Hg²⁺ ions occurred, thus forming the Ag–Hg state. These obtained results agree with the previous literature in forming the Ag–Hg phase [28]. The stability and contacting effects for each AgNPs@AG and formatted Ag–Hg solutions with ambient conditions were evaluated for more support. The process was performed by opening the bottle head at different times (24 to 240 h), as shown in Figure 2b (black line). The fabricated sensor recorded no notable change in color or their stability to produce another state, indicating the perfect role of the gum in protecting the silver nanoparticles and using it for long periods.

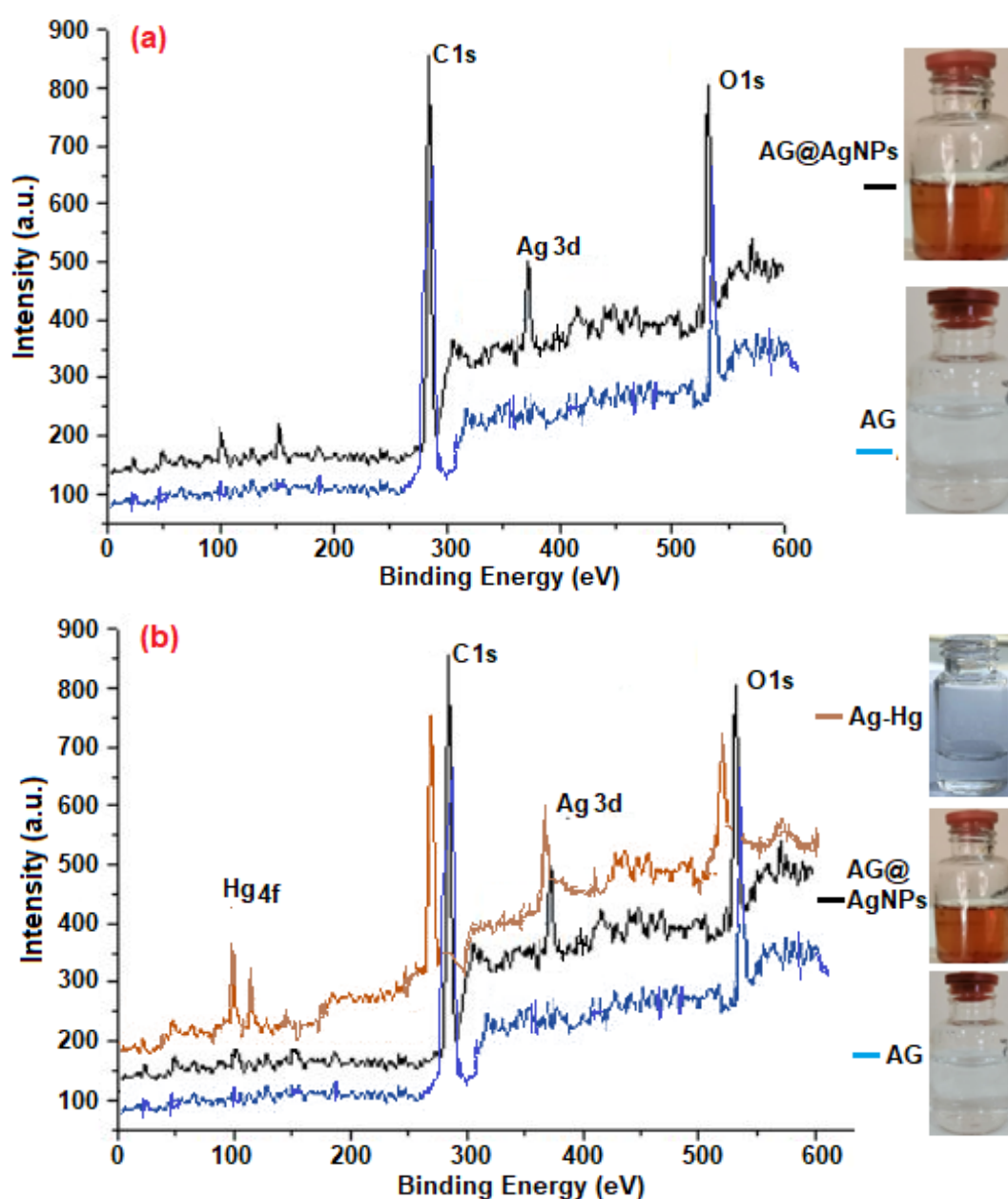


Figure 2. (a) XPs spectra of AG and AgNPs@AG; (b) XPs analysis of AG, AgNPs@AG, and Ag–Hg.

2.4. XRD Measurement

XRD is a unique tool used to determine the crystalline structure of the fabricated materials at different scales. However, XRD analysis has been applied for each AG, AgNPs@AG, and Ag–Hg. The spectrum line pattern of AG (black line) revealed a significant broad peak located at 2θ , 20° , which assumed back to the polysaccharide present in the gum composition [29]. This value was recorded besides the formation of AgNPs, after they encapsulated the AgNPs, where the analysis spectrum of AgNPs@AG (brown line) revealed excellent four peaks localized at 2θ values of 38.27° , 44.48° , 64.59° , and 77.46° , respectively, which had the corresponding planes (hkl) (111), (200), (220), and (311), respectively, as shown in Figure 3. The recorded results confirmed that the prepared AgNPs@AG possessed face-centered cubic lattices [15]. The appearance of sharp peaks in the X-ray spectrum at the base level strongly indicated that the synthesized AgNPs were prepared in a good form. The average size (D) for the as-prepared AgNPs@AG was calculated by employing the Scherrer equation ($D = [0.9\lambda / \beta \cos\theta]$), where λ and β represent the wavelength source and the breadth of the diffraction line at its half intensity maximum recorded in XRD spectrum, respectively. The calculations showed that the average size of the prepared AgNPs@AG crystalline was found to be 19 nm. However, after treating the prepared sensor with the sample of mercury ions, the XRD spectrum pattern (blue line) recorded the absence of AgNPs@AG peaks with the appearance of new interesting sharp peaks at locations 25.79° , 32.51° , 56.26° , and 66.11° , which returned to the formation of the Ag–Hg status. These measured values agree with the previous work's results [30].

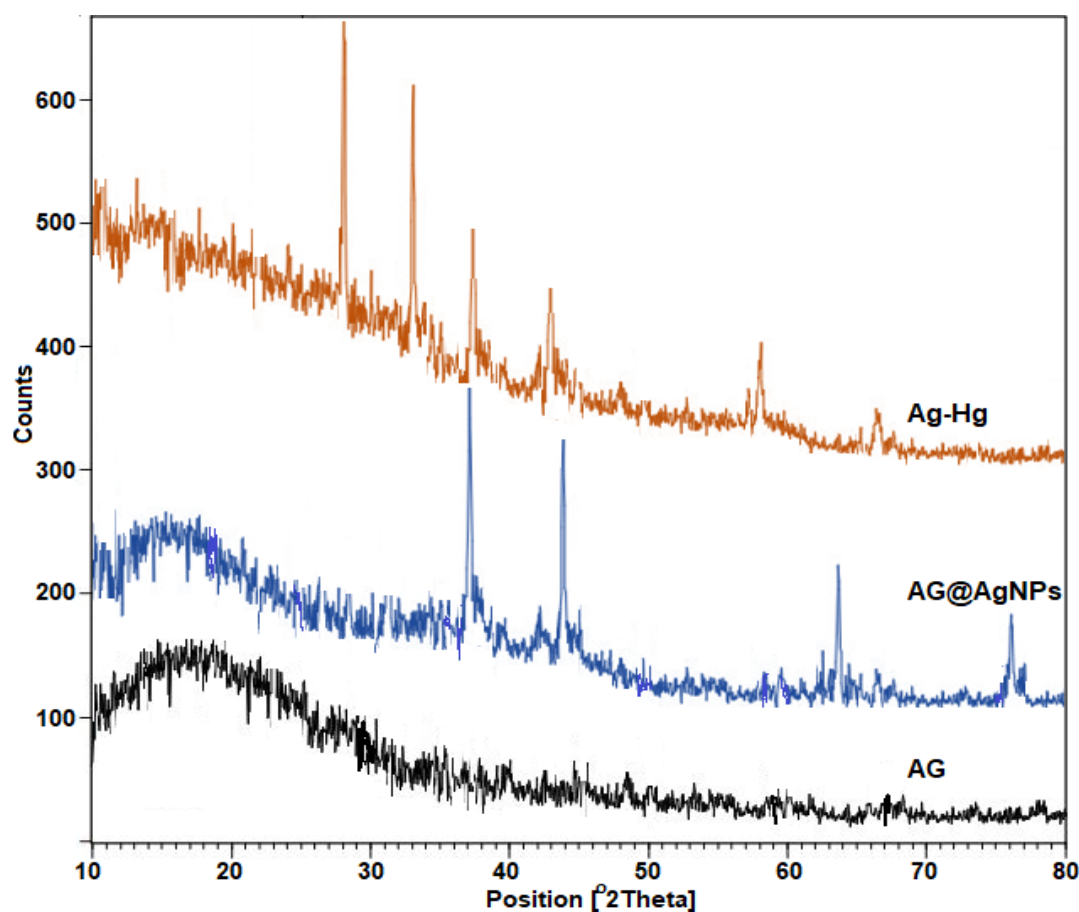


Figure 3. XRD studies of AG (black line), AgNPs@AG (blue line), and Ag–Hg (brown line).

2.5. FESEM and HR-TEM Photograph Analysis

The external and internal structures of the prepared nanoparticles has been explored and determined by FESEM and HR-TEM microanalysis. It is essential for its contribution to characterizing the particle type involved in the colorimetric response process. The analysis of FE-SEM photos (Figure 4a) revealed that AgNPs@AG formed in tiny and nonagglomerated spherical shapes due to the oily biomass nature of the gum extract. In addition, the image analysis (Figure 4b) revealed that the AgNPs@AG particles formed with perfect sizes ranging from 15 to 17 nm, which indicated the efficiency of the bio fabrication method. However, after adding these small nanosize AgNPs to the Hg ions sample, FESEM images showed excellent aggregation of precipitate, attributed to the formation of Ag–Hg (Figure 4c). The formation of the mercury–silver state occurred through the adsorption of mercury ions on the active surface of the AgNPs. Further, it could be due to its adhesion to the resin covering the AgNPs surface, which then interacted with the active AgNPs. There was a consistent parallel agreement between the images acquired from the HR-TEM and the data collected from the FESEM regarding the formation of small nanosphere particles. (Figure 4d). In contrast, Figure 4e proved the good trapping of mercury ions by the sensor with perfect aggregation. XRD and XPs have confirmed this hypothesis analysis results, in addition to the results and explanations of the published research.

2.6. EDS and EDC Identification

Synthesizing and producing good, clean, cheap, and sustainable sensors using green methods for colorimetric response is considered one of the most important challenges for researchers. For this purpose, the purity of fabricated AgNPs@AG was evaluated by determining their components using elements distribution spectroscopy (EDS) supported by elements spread diagram (ESD). The EDS spectrum (Figure 5a) revealed good weights ratios of elements for silver (Ag = 34.2%), oxygen (O = 17.5%), and carbon (C = 47.4%). No emergence or recording of other elements in the EDS chart is strong evidence of the clean methodology for this process. However, this advantage was exploited for the detection of Hg ions by the prepared sensor, where the analysis revealed the excellent formation of the Ag–Hg compound with ratios of 45, 67, 77, and 98, which belonged to the Ag, O, C and Hg, respectively (Figure 5b). EDS analysis clearly supported the XRD, XPs, FESEM, and HR-TEM analysis results, as it proved that the agglomeration of components and the formation of the Ag–Hg structure were due to the role of the bio-active surface of AgNPs and their resin coating that acted as a linking and reducing agent.

2.7. Factors Affecting the Sensing Process

2.7.1. Effect of pH on the Reaction Medium

It was recorded that the pH of AgNPs@AG was slightly acidic (6.1). This could promote that the as-prepared silver nanosensor was coated with proton donor functional groups such as hydroxyl, carboxyl, and carbonyl groups, which remarkably exist in carbohydrate molecules mentioned in almond gum constituents [31]. However, by examining the impact of acidity and basicity on the medium of the reaction, we observed that the absorbance value of the mixture was increased. This could be attributed to the formation of turbidity. Moreover, the assumed reason we expected was the presence of a small percentage of protein participating in the capping process of silver nanoparticles. However, the optimum pH of the mixture was assigned at 6.1, as shown in Figure 6.

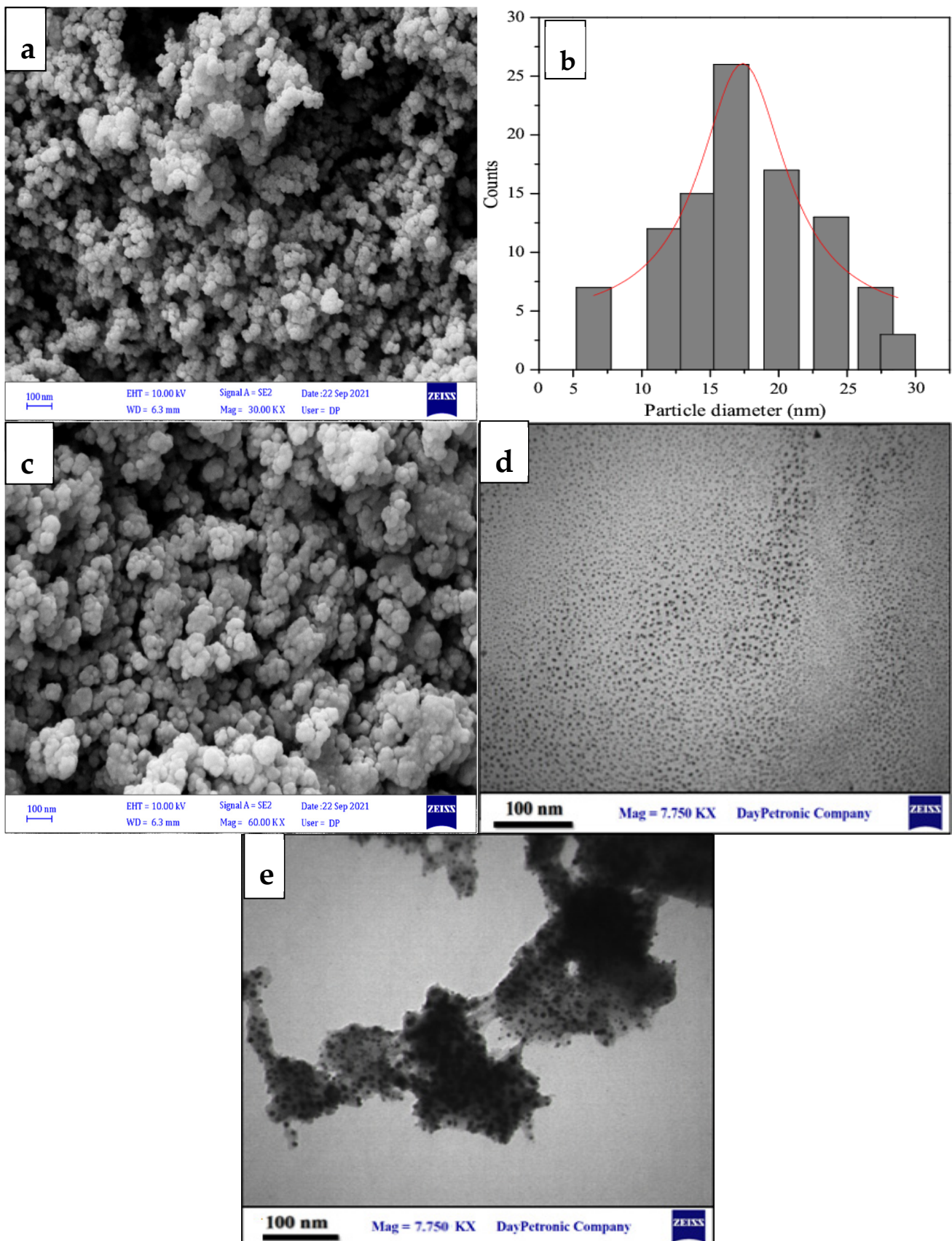


Figure 4. FESEM images of AgNPs@AG and size distribution (a,b) and Ag-Hg (c); HR-TEM images of AgNPs@AG (d) and Ag-Hg (e).

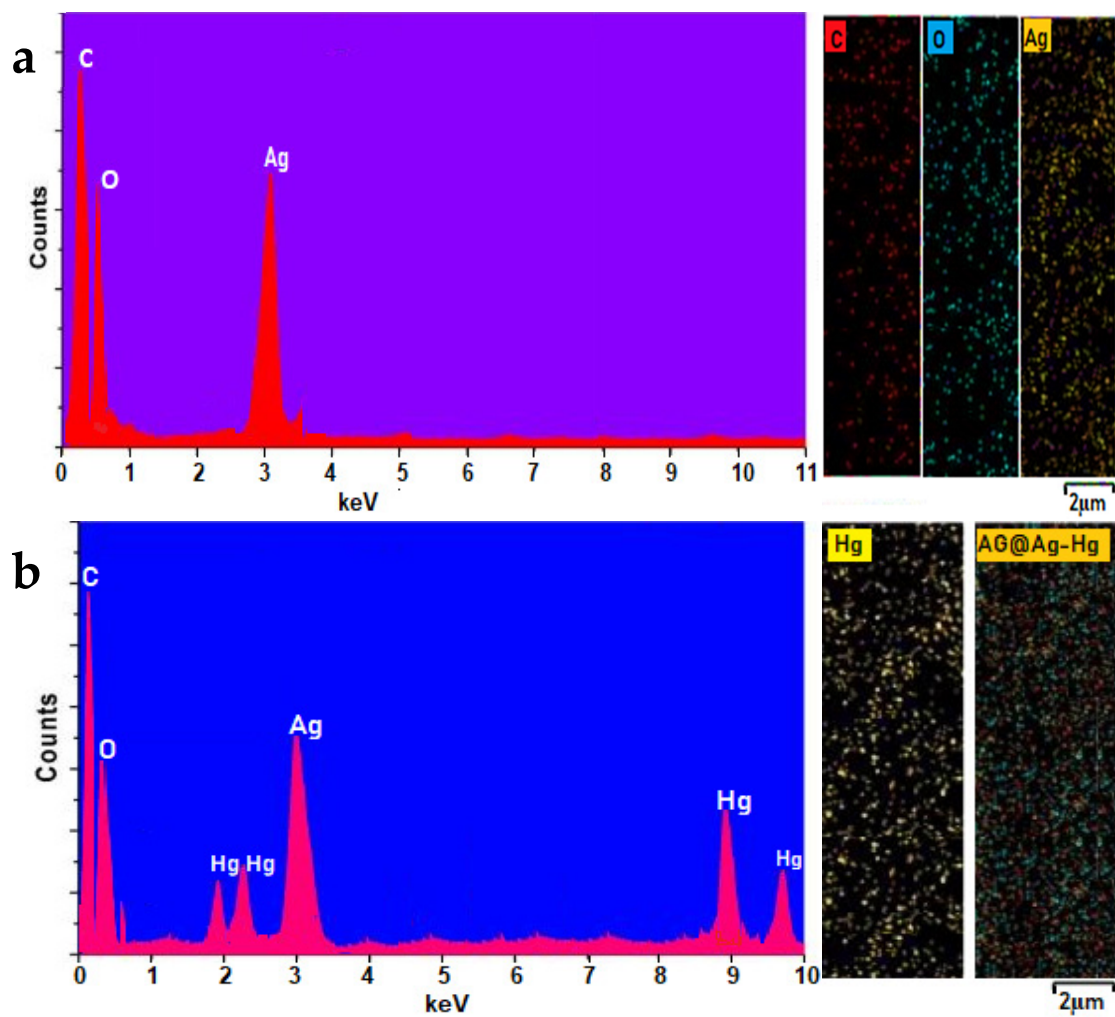


Figure 5. EDS measurements of AgNPs@AG supported with ESD (a) and Ag–Hg with supported ESD (b).

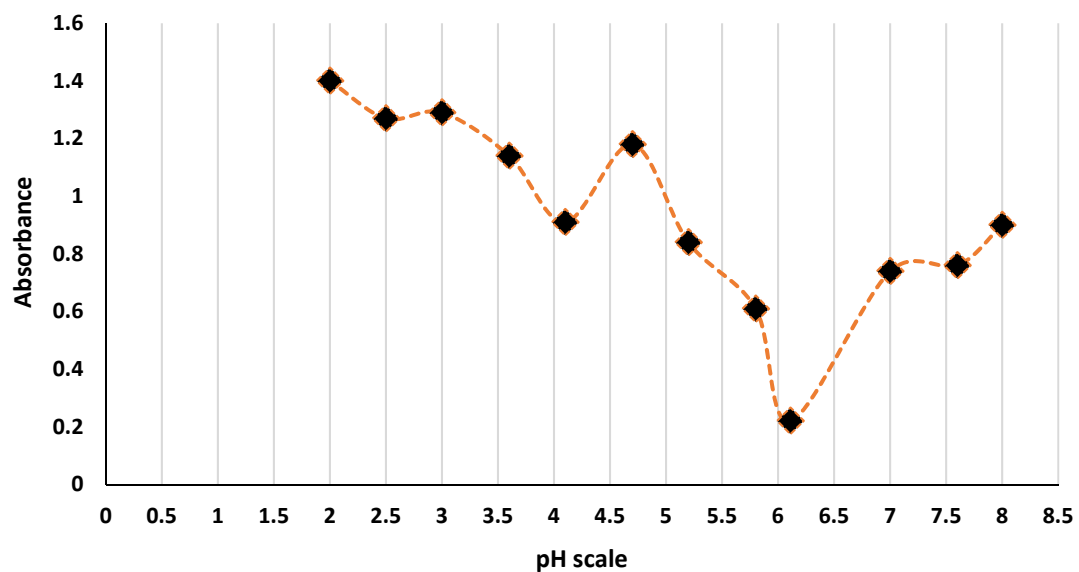


Figure 6. pH scale and its effect on the AgNPs@AG reaction medium.

2.7.2. Calibration Curve of the Method

The validity of the method was examined after standardizing the optimum conditions. The change in ΔA value of AgNPs@AG was monitored at 410 nm (Figure 7a) upon mixing the silver nanosensor with Hg^{2+} ions. The method observed good linearity achieved over a concentration range of 10–180 mg/L (see Figure 7b) by plotting the absorbance values against Hg^{2+} concentrations. Further, the correlation of determination (R^2) was 0.989. Therefore, the limit of detection (LOD) was 0.5 mg/L, and the limit of quantification (LOQ) was calculated to be 1.69 mg/L. The limit of detection (LOD) and the limit of quantification (LOQ) were determined from the equation ($3 \sigma/\text{slope}$) and ($10 \sigma/\text{slope}$), respectively.

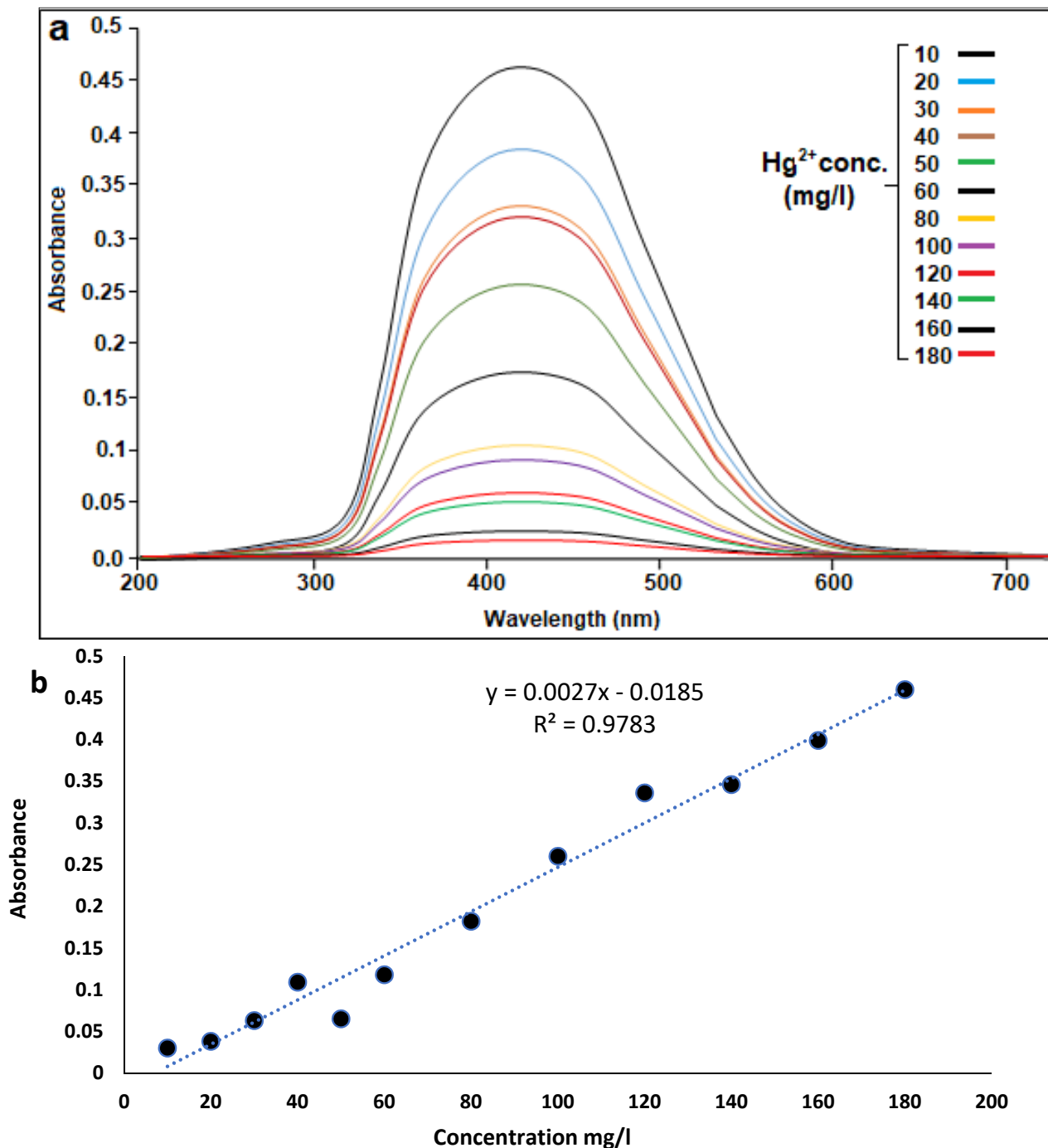


Figure 7. UV–Vis analysis (a) and calibration calculation (b) of AgNPs@AG performance validity at different concentrations (10–180 mg/L).

2.7.3. Effect of Time on the Sensing Process

The time effect was studied by monitoring the color change of AgNPs@AG from yellow color to colorless. Further, the sensing behavior was tracked using a spectrophotometer following the decreasing absorbance value against blank. It was shown that the sensing of mercury ions in an aqueous medium by silver nanoparticles was very rapid and the yellow color of AgNPs@AG disappeared instantly after the addition of silver nanoparticles with Hg^{2+} ions. The recorded time for this action was 30 s, indicating that the sensing process was swift and efficient.

2.7.4. Comparative Study between AgNPs@AG and Other Catalysts in Hg Detection

Comparing and evaluating the preparation approach, ease of conduct, and activity of any newly prepared catalyst with previously synthesized catalysts is crucial to achieving the same purpose. Here, the activity and efficiency of our fabricated sensor based on the LSPR of AgNPs@AG to detect Hg^{2+} ions were compared with those obtained by previous methods and works (Table 1). Furthermore, the prepared catalyst was compared with many different nano metallic sensors for detecting Hg^{2+} ions. The comparison table shows that our novel fabricated AgNPs@AG revealed good results for Hg^{2+} ions detection compared to the different synthesized green sensors and chemically synthesized ones. The good benefits of AgNPs@AG sensor are represented in the quick sensing of Hg^{2+} ion with the color change and noticing it with the naked eye in a short time. This result confirmed that the surface of our catalyst had excellent activity. In addition, it had high efficiency with low cost and was environment-friendly. Another advantage was that our procedure for estimating Hg^{2+} ions was compared with the different approaches. The recorded data for our work principle proved that it is easy to perform, sensitive, and cheap without needing any further enhancement or using large complex apparatuses or relatively complex detection steps that need a long time.

Table 1. Comparison of AgNPs@AG activity against detection of mercury (Hg^{2+}) with the previous published literature and reports.

No.	Principles and Sensor Used	Target Ion	Limit of Detection (LOD)	Limit Time	Reference
(A) Greenly synthesized					
1	Spectrophotometry: AgNPs	Mercury	16×10^{-2} mg/L	-	[32]
2	Spectrophotometry: AgNPs	Mercury	44×10^{-2} mg/L	5 min	[33]
3	Spectrophotometry: AgNPs	Mercury	74×10^{-7} mg/L	20 min	[34]
4	Spectrophotometry: AgNPs	Mercury	8×10^{-6} mg/L	5 min	[35]
(B) Chemically synthesized					
5	Spectrophotometry: Ag NPs	Mercury	16×10^{-4} mg/L	6 min	[36]
6	Spectrophotometry: Ag NPs	Mercury	6×10^{-1} mg/L	8 min	[37]
(C) Other nano metals					
7	Spectrophotometry: Au NPs	Mercury	2×10^{-4} mg/L	10 min	[38]
8	Spectrophotometry: Pt NPs	Mercury	7×10^{-5} mg/L	30 min	[39]
(D) Other principles					
9	HPLC	Mercury	8×10^{-4} mg/L	12 min	[40]
10	Electrochemistry	Mercury	12×10^{-3} mg/L	1.5 min	[41]
11	Electrophoresis	Mercury	1.4 mg/L	5 min	[42]
12	Fluorimetry	Mercury	8.4×10^{-5} mg/L	5min	[43]
13	GC-FI	Mercury	1×10^{-5} mg/L	60 min	[44]
14	Amperometry	Mercury	2×10^{-6} mg/L	1 min	[45]
15	AgNPs@AG: Spectrophotometry	Mercury	5×10^{-1} mg/L	30 s	This work

2.8. Evaluation of the Sensor Selectivity

The performance sensitivity, selectivity, and the naked eye noticeable for AgNPs@AG sensor against groups of different anions and cations were evaluated. The test was performed with the same optimum conditions (a mixture of 3 mL Hg^{2+} and 50 μL of AgNPs@AG) against several cations and anions. The recommended method was tracked to evaluate the effect of the interferences on determining the Hg^{2+} ions. However, interferences for I^- , Cl^- , Na^+ , and Li^+ were at 1000 ppm and those for Mg^{2+} , Ba^{2+} , and NO_3^- were at 250 ppm, whereas interferences for Zn^{2+} , Fe^{2+} and Co^{2+} were at 50 ppm. For adequate consideration, an error of 5% in concentration was recorded. The sensor behavior against mercury ions revealed excellent yellow color with a clear naked eye seen (Figure 8a). In contrast, the foreign ions did not overlap with the required ion (Hg ions) during the sensing process, even with the high concentrations, with no color change. However, based on the monitoring process of the reaction mixture by the naked eye (Figure 8a), no change in the yellow color solution was observed in less than 13 seconds and even 10 minutes for the common ions of Zn^{2+} , Co^{2+} , Fe^{2+} , Mg^{2+} , Ba^{2+} , Na^+ , K^+ , I^- , Cl^- , and NO_3^- even at concentrations 500 times higher than for mercury. UV–Vis analysis supported this behavior more (Figure 8b,c). The variation detail of UV–Vis measurements revealed that the sensor's selectivity worked only with mercury ions with a significant change in the absorbance curve, ranging from 0 to 0.19 nm. In contrast, the analysis revealed low absorbance changes with the other ions (Zn^{2+} , Co^{2+} , Fe^{2+} , Mg^{2+} , Ba^{2+} , Na^+ , Li^+ , I^- , Cl^- , and NO_3^- for the ranges of 0.01, 0.03, 0.02, 0.04, 0.04, 0.04, 0.02, 0.04, 0.04, and 0.05 nm, respectively). The results confirmed that this novel sensor had excellent detection performance for mercury ions in the effluent.

2.9. Performance of the AgNPs@AG Sensor in Tap Water Samples

In this part, the performance of the developed AgNPs@AG sensor was evaluated by utilizing it with collected actual water samples for the detection and determination of mercury ions. Water samples (home drinking water) were collected from different places in Shekan area in Duhok city and in Kurdistan region in Iraq during different times. This test was performed to prove the reliability of the efficient colorimetric detection response method of the AgNPs@AG sensor in practical applications. First, the principle of pretreatment for water samples was applied according to the protocol of Section 2.4. According to the obtained data in Table 2, it was reported that the sensor behavior revealed no color transformation with the samples of tap water (i.e., before dealing it with mercury ions) even with high addition concentrations of the sensor. Furthermore, it indicated no mercury ions in tap water samples or overlapping water total contents with the sensor solution. In contrast, after the treatment of the same water samples with mercury ions, the recovery experiments for mercury ions were carried out, and the results were recorded as shown in Table 2. The recovery process results revealed that the prepared silver catalyst had good recovery activity for mercury ions and with ratios of 91.5–101.7% at different concentrations (10–50 ppm), which proved that the presented method is feasible for the mercury ions detection in real environmental water samples.

Table 2. Detection of Hg ions in real water samples.

Sample	Added Analyte (mg/L)	Found (mg/L)	Recovery Ratios * (% , $n = 3$)
Before treatment	0	0	0
After treatment	10	9.1	91 ± 0.89
	20	19.4	97 ± 1.59
	30	29.7	99 ± 0.67
	40	40.2	100.5 ± 0.93
	50	50.7	101.7 ± 1.88

* Mean ± standard deviation ($n = 3$).

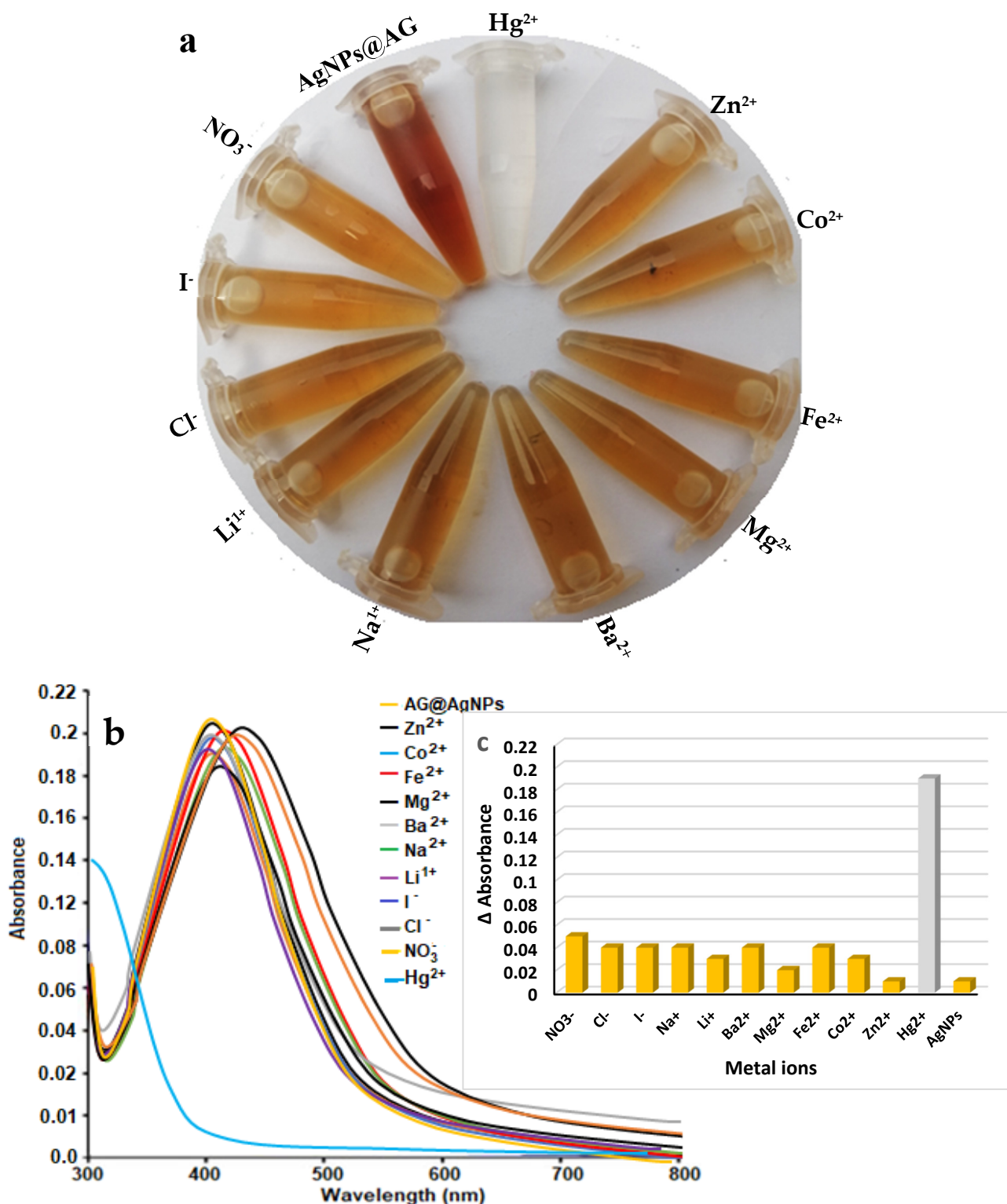
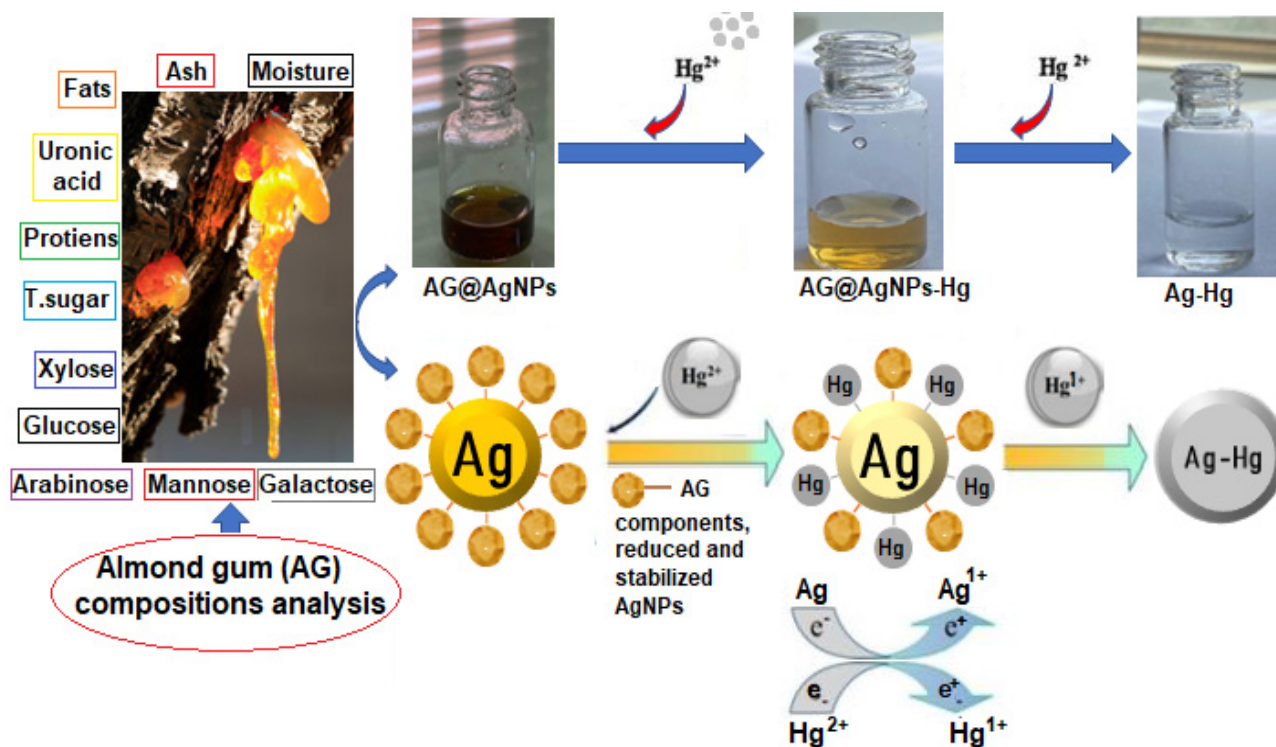


Figure 8. (a) Photo of the AgNPs@AG sensor performance against different groups of anions and cations; (b) absorbances of anionic and cationic foreign ions at certain wavelengths; (c) absorbance of different anions and cations at different wavelengths.

2.10. Assumed Colorimetric Response of AgNPs@AG against Hg^{2+} Ions

The proposed mechanism for the response of the as-prepared nano silver catalyst (AgNPs@AG) against sensing and detection of mercury ions [Hg^{2+}] is predicted, as the illustrated pathway (Scheme 2): firstly, mercury ion [Hg^{2+}] coordinates with almond gum

by hydroxyl [–OH] and carboxylic [–CO₂H] groups, as confirmed and proved by the XPs study, leading to the formation of Hg–almond gum complex. Furthermore, during an increase in Hg²⁺ ion concentration, Hg²⁺ ions quickly adsorb on the active surface of the AgNPs, after the redox reaction between Ag⁰ and Hg²⁺ and production of Ag⁺ and Hg⁺. After that, the state of Ag⁰ is changed to the Ag⁺ state through the electron transfer process from almond gum to Ag⁺, thus initializing the process between both Ag⁺ and Hg⁺ to form of the Ag–Hg phase. Therefore, in this process, almond gum plays a significant role in reducing, stabilizing, and being a good electron donor in preparation for each AgNP and Ag–Hg state. Furthermore, the electron transmission from almond gum to Ag⁺ gains support from the suggested synthetic procedure without additional reducing agents used during the AgNPs fabrication [30]. The fabrication of AgNPs@AG and the formation of Ag–Hg were confirmed and supported by UV–Vis measurement, XRD study, XPs analysis, and an increase in the nanoparticles' sizes for both silver nanoparticles and the amalgamate that appeared by the FESEM and HR-TEM images analysis. The increase in nanoparticle size was due to the well-active surface of the prepared NPs, causing perfect agglomeration and a “swelling effect” that occurs, which is attributed to the diffusion of Hg atoms, thus increasing the total nanoparticle sizes. Another vital piece of evidence, the high decrease in the wavelength value of AgNPs@AG at a constant position (410 nm) at the addition of mercury ions, could be attributed to the displacement of almond gum on the AgNPs surface by mercury ions due to the higher affinity of Ag toward the Hg ions. Hence, this leads to the fabrication of Ag–Hg with the aqueous phase.



Scheme 2. Assumed colorimetric response of AgNPs@AG against Hg²⁺ ions.

3. Methodology

3.1. Materials and Methods

All chemical materials were pure-grade analytical reagents, including silver nitrate (AgNO₃, FW = 169.87 g/mol, CAS No: 7761-88-8MP) and sodium hydroxide (NaOH, FW = 40 g/mol, CAS No:1310-73-2), which were provided from Scharlue comp. in Barcelona Spain.

A healthy almond gum was collected from Charboot village, Zeebar district in Akre and Duhok–Kurdistan region of Iraq in August 2021. A mercury chloride stock solution

(100 mg/L) was prepared daily due to dissolving a certain weight of mercury chloride salt in distilled water. The stock solution of mercury chloride was then stored in a dark container in a cool place for the subsequent experiments. All experiments were performed in the laboratory under ambient conditions.

3.2. Preparation of the Almond Gum Solution

The solution of 1% almond gum was prepared following these steps. First, the solid particles of almond gum were crushed to a fine powder by a mortar. Next, 1 g of the gum powder was transferred to a conical flask, dissolved with 100 mL distilled water and stirred vigorously at 50 °C for 30 min. Finally, the mixture was filtered with a gauze and a filter paper to separate insoluble solid fractions and stored in a refrigerator at 2 °C to be used for the reduction process of silver ions.

3.3. Fabrication of Silver Nanoparticles (AgNPs@AG)

The synthesis process included mixing 3 mL of a 0.1 M AgNO₃ solution with 25 µL of 0.3 M NaOH. The mixture was stirred at 70 °C for 20 min. Afterwards, 2 mL of 1% almond gum solution were added to the mixture, followed by stirring for 45 min. A yellow–brown color appeared 15 min after the addition of the almond gum solution. The yellow–brown color continuously developed, until the whole mixture became brown, indicating the reduction process of silver ions and the formation of silver nanoparticles.

3.4. Detection of Hg²⁺ Ions by AgNPs@AG

An easy and short procedure was conducted to investigate the efficiency of AgNPs@AG as a rapid colorimetric sensor to detect mercury ions in an aqueous solution. A group of 5 mL glass vials was arranged and filled with 3 mL of different concentrations of mercury ions (10, 20, 30, 40, 50, 60, 70, 80, 90, and 100 mg/L). It was shown that the yellow color of AgNPs@AG disappeared rapidly after each addition of silver nanoparticles to the mercury solution, indicating that AgNPs@AG worked as an efficient probe against mercury ions in an aqueous solution. The procedure was monitored by a UV–Vis device to follow the decrease in absorbance at 410 nm to confirm the sensing process.

3.5. Detection of Mercury Ions in Real Water Samples

Various drinking water samples were collected from different locations in Shekhan District and Duhok in Iraq. The sensing of mercury ions in real water samples was conducted according to the optimum conditions of the procedure.

3.6. Diagnosis Techniques Used

The synthesized AgNPs@AG sensor was diagnosed with several techniques, including using an ultraviolet–visible (UV–Vis) spectrophotometer (nanodrop 2000/2000 c) to record the predicted LSPR band for the brown–yellow solution of AgNPs. X-ray diffraction (XRD) measurement was performed for AgNPs@AG by a PAN analytical X'PERT PRO model X-ray diffractometer operated at 30 kV and 45 mA, to reveal the crystalline nature of AgNPs@AG. The chemical surface nature of AgNPs@AG was diagnosed with an X-ray photoelectron spectroscopy (XPS) tool (PHI 5000 Versa Prob II: Supplier Model, Japan), supported with an Al anode set at 140 W and operated at a pass energy of 50 eV. Field-emission scanning electron microscopy (FESEM) analysis (SEM-ZEISS-Singapore, Malaysia) with an accelerating voltage of 20 kV, supported with energy-dispersive spectroscopy (EDS) measurement, was used to predict the shape nature of the prepared nanoparticles. High-resolution-transmission electron microscopy (HR-TEM) measurements were carried out for AgNPs@AG by a JOEL apparatus (model 1200 EX; Cu grid), with an accelerating voltage of 40 kV, supported with a elements spread diagram (ESD) using (ZEISS-TEM instrument), operating at a 200 magnification.

4. Conclusions

In this study, silver nanoparticles have been synthesized employing a green strategy at ambient conditions. Natural exudate (almond gum) has been used as a reducing and stabilizing agent in order to produce a stable silver nanostructure. The distinctive optical properties and sensing behaviors of the as-prepared silver nanoparticles were observed due to reaction with mercury ions (Hg^{2+}) in an aqueous solution. Rapid and high sensitivity have been reported when mixing the silver nanosensor with a proper quantity of the target ions. In addition, it has been shown that the synthesized silver nanoparticles were stable and lasted for two months and no decolorization was observed.

Author Contributions: S.Y.S.Z.: conceiving the main idea, writing, and results analysis; A.Y.S.Z.: conceptualization, writing, and results analysis; O.I.H.: writing and editing; D.A.H.: viewing and editing; E.H.H.: viewing and editing. All authors have read and agreed to the published version of the manuscript.

Funding: This research received no external funding.

Data Availability Statement: All data and details regarding the work of this original article have been provided in this paper without further information.

Conflicts of Interest: The authors declare that there is no conflict of interest or any personal circumstances or interest that may be perceived as inappropriately influencing the representation or interpretation of reported research results.

References

1. Alshawi, J.M.S.; Mohammed, M.Q.; Alesary, H.F.; Ismail, H.K.; Barton, S. Voltammetric Determination of Hg^{2+} , Zn^{2+} , and Pb^{2+} Ions Using a PEDOT/NTA-Modified Electrode. *ACS Omega* **2022**, *7*, 20405–20419. [[CrossRef](#)] [[PubMed](#)]
2. Mohammed, M.Q.; Ismail, H.K.; Alesary, H.F.; Barton, S. Use of a Schiff base-modified conducting polymer electrode for electrochemical assay of Cd(II) and Pb(II) ions by square wave voltammetry. *Chem. Pap.* **2022**, *76*, 715–729. [[CrossRef](#)]
3. Ali, L.I.A.; Ismail, H.K.; Alesary, H.F.; Aboul-Enein, H.Y. A nanocomposite based on polyaniline, nickel and manganese oxides for dye removal from aqueous solutions. *Int. J. Environ. Sci. Technol.* **2021**, *18*, 2031–2050. [[CrossRef](#)]
4. Ismail, H.K.; Ali, L.I.A.; Alesary, H.F.; Nile, B.K.; Barton, S. Synthesis of a poly(p-aminophenol)/starch/graphene oxide ternary nanocomposite for removal of methylene blue dye from aqueous solution. *J. Polym. Res.* **2022**, *29*, 159. [[CrossRef](#)]
5. Pomal, N.C.; Bhatt, K.D.; Modi, K.M.; Desai, A.L.; Patel, N.P.; Kongor, A.; Kolivoška, V. Functionalized Silver Nanoparticles as Colorimetric and Fluorimetric Sensor for Environmentally Toxic Mercury Ions: An Overview. *J. Fluoresc.* **2021**, *31*, 635–649. [[CrossRef](#)]
6. Suvarapu, L.N.; Baek, S.O. Recent Studies on the Speciation and Determination of Mercury in Different Environmental Matrices Using Various Analytical Techniques. *Int. J. Anal. Chem.* **2017**, *2017*, 1–27. [[CrossRef](#)] [[PubMed](#)]
7. Sarkar, P.K.; Polley, N.; Chakrabarti, S.; Lemmens, P.; Pal, S.K. Nanosurface Energy Transfer Based Highly Selective and Ultrasensitive “turn on” Fluorescence Mercury Sensor. *ACS Sens.* **2016**, *1*, 789–797. [[CrossRef](#)]
8. Yasin, S.A.; Abbas, J.A.; Ali, M.M.; Saeed, I.A.; Ahmed, I.H. Methylene blue photocatalytic degradation by TiO_2 nanoparticles supported on PET nanofibres. *Mater. Today Proc.* **2020**, *20*, 482–487. [[CrossRef](#)]
9. Tauran, Y.; Brioude, A.; Coleman, A.W.; Rhimi, M.; Kim, B. Molecular recognition by gold, silver and copper nanoparticles. *World J. Biol. Chem.* **2013**, *4*, 35. [[CrossRef](#)]
10. Sabri, M.A.; Umer, A.; Awan, G.H.; Hassan, M.F.; Hasnain, A. Selection of suitable biological method for the synthesis of silver nanoparticles. *Nanomater. Nanotechnol.* **2016**, *6*, 1–20. [[CrossRef](#)]
11. Naidoo, S.; Külheim, C.; Zwart, L.; Mangwanda, R.; Oates, C.N.; Visser, E.A.; Wilken, F.E.; Mamni, T.B.; Myburg, A.A. Uncovering the defence responses of eucalyptus to pests and pathogens in the genomics age. *Tree Physiol.* **2014**, *34*, 931–943. [[CrossRef](#)]
12. Mahfoudhi, N.; Chouaibi, M.; Donsi, F.; Ferrari, G.; Hamdi, S. Chemical composition and functional properties of gum exudates from the trunk of the almond tree (*Prunus dulcis*). *Food Sci. Technol. Int.* **2012**, *18*, 241–250. [[CrossRef](#)] [[PubMed](#)]
13. Mumtaz, A.; Munir, H.; Zubair, M.T.; Arif, M.H. Mimosa pudica gum based nanoparticles development, characterization, and evaluation for their mutagenicity, cytotoxicity and antimicrobial activity. *Mater. Res. Express* **2019**, *6*, 105308. [[CrossRef](#)]
14. Kora, A.J.; Arunachalam, J. Green fabrication of silver nanoparticles by gum tragacanth (*Astragalus gummifer*): A dual functional reductant and stabilizer. *J. Nanomater.* **2012**, *2012*, 69. [[CrossRef](#)]
15. Venkatesham, M.; Ayodhya, D.; Madhusudhan, A.; Veerabhadram, G. Synthesis of stable silver nanoparticles using gum acacia as reducing and stabilizing agent and study of its microbial properties: A novel green approach. *Int. J. Green Nanotechnol. Biomed.* **2012**, *4*, 199–206. [[CrossRef](#)]

16. El-Adawy, M.M.; Eissa, A.E.; Shaalan, M.; Ahmed, A.A.; Younis, N.A.; Ismail, M.M.; Abdelsalam, M. Green synthesis and physical properties of Gum Arabic-silver nanoparticles and its antibacterial efficacy against fish bacterial pathogens. *Aquac. Res.* **2021**, *52*, 1247–1254. [[CrossRef](#)]
17. Quelemes, P.V.; Araruna, F.B.; de Faria, B.E.F.; Kuckelhaus, S.A.S.; da Silva, D.A.; Mendonça, R.Z.; Eiras, C.; Soares, M.J.d.S.; Leite, J.R.S.A. Development and antibacterial activity of cashew gum-based silver nanoparticles. *Int. J. Mol. Sci.* **2013**, *14*, 4969–4981. [[CrossRef](#)]
18. Kora, A.J.; Sashidhar, R.B. Antibacterial activity of biogenic silver nanoparticles synthesized with gum ghatti and gum olibanum: A comparative study. *J. Antibiot.* **2015**, *68*, 88–97. [[CrossRef](#)]
19. Venkatesham, M.; Ayodhya, D.; Madhusudhan, A.; Santoshi Kumari, A.; Veerabhadram, G.; Girija Mangatayaru, K. A Novel Green Synthesis of Silver Nanoparticles Using Gum Karaya: Characterization, Antimicrobial and Catalytic Activity Studies. *J. Clust. Sci.* **2014**, *25*, 409–422. [[CrossRef](#)]
20. Samrot, A.V.; Angalene, J.L.A.; Roshini, S.M.; Raji, P.; Stefi, S.M.; Preethi, R.; Selvarani, A.J.; Madankumar, A. Bioactivity and Heavy Metal Removal Using Plant Gum Mediated Green Synthesized Silver Nanoparticles. *J. Clust. Sci.* **2019**, *30*, 1599–1610. [[CrossRef](#)]
21. Rezaei, A.; Nasirpour, A.; Tavanai, H. Fractionation and some physicochemical properties of almond gum (*Amygdalus communis* L.) exudates. *Food Hydrocoll.* **2016**, *60*, 461–469. [[CrossRef](#)]
22. Yaseen Sharaf Zeebaree, A.; Yaseen Sharaf Zeebaree, S.; Rashid, R.F.; Ismail Haji Zebari, O.; Albarwry, A.J.S.; Ali, A.F.; Yaseen Sharaf Zebari, A. Sustainable engineering of plant-synthesized TiO₂ nanocatalysts: Diagnosis, properties and their photocatalytic performance in removing of methylene blue dye from effluent. A review. *Curr. Res. Green Sustain. Chem.* **2022**, *5*, 100312. [[CrossRef](#)]
23. Roy, K.; Sarkar, C.K.; Ghosh, C.K. Rapid colorimetric detection of Hg²⁺ ion by green silver nanoparticles synthesized using Dahlia pinnata leaf extract. *Green Process. Synth.* **2015**, *4*, 455–461. [[CrossRef](#)]
24. Kumar, V.; Singh, D.K.; Mohan, S.; Bano, D.; Gundampati, R.K.; Hasan, S.H. Green synthesis of silver nanoparticle for the selective and sensitive colorimetric detection of mercury (II) ion. *J. Photochem. Photobiol. B Biol.* **2017**, *168*, 67–77. [[CrossRef](#)] [[PubMed](#)]
25. Firdaus, M.L.; Itriani, I.F.; Yantuti, S.W.; Artati, Y.W.H.; Haydarov, R.K.; Calister, J.A.M.; Bata, H.O.; Amo, T.G. Colorimetric Detection of Mercury (II) Ion in Aqueous Solution Using Silver Nanoparticle. *Anal. Sci.* **2017**, *8*, 831–837. [[CrossRef](#)]
26. Abu-Dalo, M.A.; Othman, A.A.; Al-Rawashdeh, N.A.F. Exudate gum from acacia trees as green corrosion inhibitor for mild steel in acidic media. *Int. J. Electrochem. Sci.* **2012**, *7*, 9303–9324.
27. Han, J.K.; Madhiiudhan, A.; Bandi, R.; Park, C.W.; Kim, J.C.; Lee, Y.K.; Lee, S.H.; Wona, J.M. Green synthesis of AgNPs using lignocellulose nanofibrils as a reducing and supporting agent. *BioResources* **2020**, *15*, 2119–2132. [[CrossRef](#)]
28. Schiesaro, I.; Burratti, L.; Meneghini, C.; Fratoddi, I.; Proposito, P.; Lim, J.; Scheu, C.; Venditti, I.; Iucci, G.; Battocchio, C. Hydrophilic Silver Nanoparticles for Hg(II) Detection in Water: Direct Evidence for Mercury-Silver Interaction. *J. Phys. Chem. C* **2020**, *124*, 25975–25983. [[CrossRef](#)]
29. Zeebaree, S.Y.S.; Ismail Haji, O.; Farooq Rashid, R.; Yasin, S.A.; Zeebaree, A.Y.S.; Albarwary, A.J.S.; Zebari, A.Y.S.; Gerjees, H.A. Novel natural exudate as a stabilizing agent for fabrication of copper nanoparticles as a colourimetric sensor to detect trace pollutant. *Surf. Interfaces* **2022**, *32*, 102131. [[CrossRef](#)]
30. Abbasi, A.; Hanif, S.; Shakir, M. Gum acacia-based silver nanoparticles as a highly selective and sensitive dual nanosensor for Hg(ii) and fluorescence turn-off sensor for S₂- and malachite green detection. *RSC Adv.* **2020**, *10*, 3137–3144. [[CrossRef](#)]
31. Bashir, M.; HariPriya, S. Assessment of physical and structural characteristics of almond gum. *Int. J. Biol. Macromol.* **2016**, *93*, 476–482. [[CrossRef](#)] [[PubMed](#)]
32. Ahmed, F.; Kabir, H.; Xiong, H. Dual Colorimetric Sensor for Hg²⁺/Pb²⁺ and an Efficient Catalyst Based on Silver Nanoparticles Mediating by the Root Extract of *Bistorta amplexicaulis*. *Front. Chem.* **2020**, *8*, 591958. [[CrossRef](#)] [[PubMed](#)]
33. Demirezen Yilmaz, D.; Aksu Demirezen, D.; Mihçioğur, H. Colorimetric detection of mercury ion using chlorophyll functionalized green silver nanoparticles in aqueous medium. *Surf. Interfaces* **2021**, *22*, 100840. [[CrossRef](#)]
34. Azimpanah, R.; Solati, Z.; Hashemi, M. Green synthesis of silver nanoparticles and their applications as colorimetric probe for determination of Fe and Hg ions. *IET Nanobiotechnology* **2018**, *12*, 673–677. [[CrossRef](#)] [[PubMed](#)]
35. Memon, R.; Memon, A.A.; Sirajuddin Balouch, A.; Memon, K.; Sherazi, S.T.H.; Chandio, A.A.; Kumar, R. Ultrasensitive colorimetric detection of Hg²⁺ in aqueous media via green synthesis by *Ziziphus mauritiana* Leaf extract-based silver nanoparticles. *Int. J. Environ. Anal. Chem.* **2020**, 1–16. [[CrossRef](#)]
36. Annadhasan, M.; Rajendiran, N. Highly selective and sensitive colorimetric detection of Hg(II) ions using green synthesized silver nanoparticles. *RSC Adv.* **2015**, *5*, 94513–94518. [[CrossRef](#)]
37. Proposito, P.; Burratti, L.; Bellingeri, A.; Protano, G.; Faleri, C.; Corsi, I.; Battocchio, C.; Iucci, G.; Tortora, L.; Secchi, V.; et al. Bifunctionalized silver nanoparticles as Hg²⁺ plasmonic sensor in water: Synthesis, characterizations, and ecosafety. *Nanomaterials* **2019**, *9*, 1353. [[CrossRef](#)]
38. Yang, M.; Yao, J.; Liu, Y.; Duan, Y. Sensitive detection of mercury (II) ion using wave length-tunable visible-emitting gold nanoclusters based on protein-templated synthesis. *J. Mater. Res.* **2014**, *29*, 2416–2424. [[CrossRef](#)]
39. Li, H.; Liu, H.; Zhang, J.; Cheng, Y.; Zhang, C.; Fei, X.; Xian, Y. Platinum Nanoparticle Encapsulated Metal-Organic Frameworks for Colorimetric Measurement and Facile Removal of Mercury(II). *ACS Appl. Mater. Interfaces* **2017**, *9*, 40716–40725. [[CrossRef](#)]

40. Ichinoki, S.; Kitahata, N.; Fujii, Y. Selective determination of mercury(II) ion in water by solvent extraction followed by reversed-phase HPLC. *J. Liq. Chromatogr. Relat. Technol.* **2004**, *27*, 1785–1798. [[CrossRef](#)]
41. Gold, G.; Nkosi, D.; Pillay, K.; Arotiba, O. Electrochemical detection of Hg(II) in water using self-assembled single walled carbon nanotube-poly(m-amino benzene sulfonic acid) on gold electrode. *Sens. Bio-Sens. Res.* **2016**, *10*, 27–33. [[CrossRef](#)]
42. Sukesan, R.; Chen, Y.; Shahim, S.; Wang, S.; Sarangadharan, I.; Wang, Y. Instant Mercury Ion Detection in Industrial Waste Water with a Microchip Using Extended Gate Field-Effect Transistors and a Portable Device. *Sensors* **2019**, *19*, 2209. [[CrossRef](#)] [[PubMed](#)]
43. Kaewprom, C.; Areerob, Y.; Oh, W. Simultaneous determination of Hg (II) and Cu (II) in water samples using fluorescence quenching sensor of N-doped and N, K co-doped graphene quantum dots. *Arab. J. Chem.* **2020**, *13*, 3714–3723. [[CrossRef](#)]
44. Sarafraz-yazdi, A.; Fatehyan, E.; Amiri, A. Determination of Mercury in Real Water Samples Using in situ Derivatization Followed by Sol-Gel—Solid-Phase Microextraction with Gas Chromatography—Flame Ionization Detection. *J. Chromatogr. Sci.* **2014**, *52*, 81–87. [[CrossRef](#)] [[PubMed](#)]
45. Gumpu, M.B.; Krishnan, U.M. Design and development of amperometric biosensor for the detection of lead and mercury ions in water matrix—A permeability approach. *Anal. Bioanal. Chem.* **2017**, *409*, 4257–4266. [[CrossRef](#)]